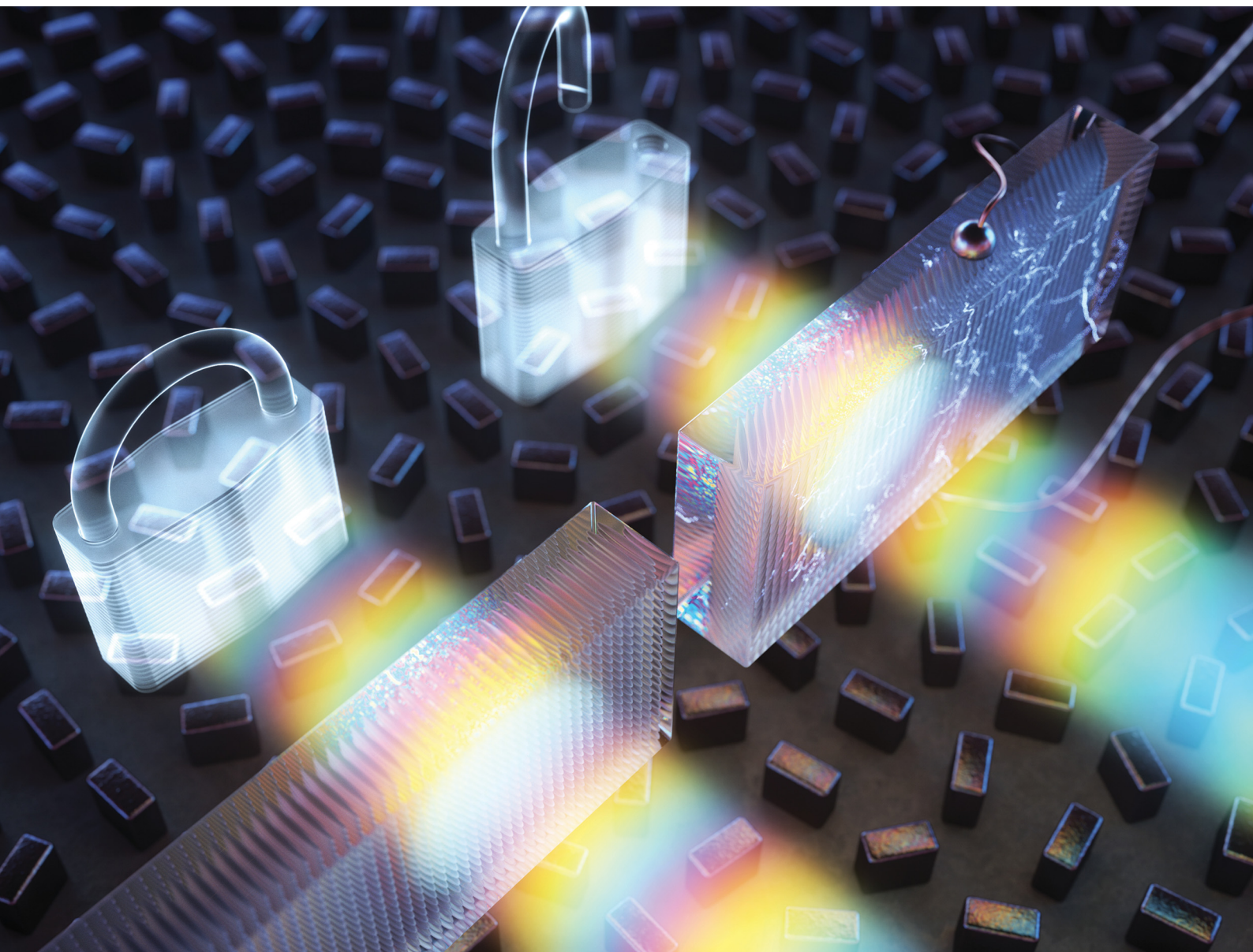# Nanoscale Horizons

The home for rapid reports of exceptional significance in nanoscience and nanotechnology

rsc.li/nanoscale-horizons

ROYAL SOCIETY
OF CHEMISTRY

COMMUNICATION
Muhammad Zubair, Muhammad Qasim Mehmood,
Yehia Massoud, Junsuk Rho *et al.*
Spin-isolated ultraviolet-visible dynamic meta-holographic
displays with liquid crystal modulators

NCNST

Nanoscale Horizons

Check for updates

Spin-isolated ultraviolet-visible dynamic meta-holographic displays with liquid crystal modulators†

Aqsa Asad,‡[a] Joohoon Kim,‡[b] Hafiz Saad Khaliq,‡[ac] Nasir Mahmood,[d] Jehan Akbar,[e] Muhammad Tariq Saeed Chani,[f] Yeseul Kim, [iD][b] Dongmin Jeon,[b] Muhammad Zubair, [iD]*[d] Muhammad Qasim Mehmood, [iD]*[a] Yehia Massoud*[d] and Junsuk Rho [iD]*[bghi]

Wearable displays or head-mounted displays (HMDs) have the ability to create a virtual image in the field of view of one or both eyes. Such displays constitute the main platform for numerous virtual reality (VR)- and augmented reality (AR)-based applications. Meta-holographic displays integrated with AR technology have potential applications in the advertising, media, and healthcare sectors. In the previous decade, dielectric metasurfaces emerged as a suitable choice for designing compact devices for highly efficient displays. However, the small conversion efficiency, narrow bandwidth, and costly fabrication procedures limit the device's functionalities. Here, we proposed a spin-isolated dielectric multi-functional metasurface operating at broadband optical wavelengths with high transmission efficiency in the ultraviolet (UV) and visible (Vis) regimes. The proposed metasurface comprised silicon nitride (Si_3N_4)-based meta-atoms with high bandgap, *i.e.*, ∼ 5.9 eV, and encoded two holographic phase profiles. Previously, the multiple pieces of holographic information incorporated in the metasurfaces using interleaved and layer stacking techniques resulted in noisy and low-efficiency outputs. A single planar metasurface integrated with a liquid crystal was demonstrated numerically and experimentally in the current work to validate the spin-isolated dynamic UV-Vis holographic information at broadband wavelengths. In our opinion, the proposed metasurface can have promising applications in healthcare, optical security encryption, anti-counterfeiting, and UV-Vis nanophotonics.

New concepts

Integrating meta-holographic displays with AR technology can have potential applications in advertising, media, and especially healthcare sectors for bio-medical imaging, training, and education. Previously, dielectric meta-nano surfaces emerged as the suitable choice for designing compact devices for highly efficient displays. However, the essential factors limiting the device functionality are low conversion efficiency, narrow bandwidth, and costly fabrication procedures. We demonstrated a spin-isolated dielectric multi-functional planar nano-surface operating at broadband optical wavelengths with high transmission efficiency in the ultraviolet (UV) and visible (Vis) regimes. The proposed nano-surface comprised silicon nitride (Si_3N_4)-based meta-atoms with a high bandgap, *i.e.*, ∼ 5.9 eV, and encoded two distinct holographic phase profiles in a single metasurface using a single engineered meta-atom. Moreover, integrating the proposed nano-surface with a liquid crystal was demonstrated numerically and experimentally to reproduce spin-isolated dynamic holographic information at broadband UV-Vis wavelengths. This research may pave the way toward designing highly efficient multi-functional meta-devices to produce dynamic next-generation UV-Vis holographic displays for promising applications in healthcare, media, smart security, and data encryption.

Introduction

The variegated design phenomena of metasurfaces to simultaneously manipulate the intrinsic properties (amplitude, polarization, and phase) of light *via* subwavelength nano-resonators, enable

[a] *MicroNano Lab, Department of Electrical Engineering, Information Technology University (ITU) of the Punjab, Lahore 54600, Pakistan. E-mail: qasim.mehmood@itu.edu.pk*

[b] *Department of Mechanical Engineering, Pohang University of Science and Technology (POSTECH), Pohang 37673, Republic of Korea. E-mail: jsrho@postech.ac.kr*

[c] *School of Electronic and Electrical Engineering, Kyungpook National University, Daegu 41566, Republic of Korea*

[d] *Innovative Technologies Laboratories (ITL), King Abdullah University of Science and Technology (KAUST), Saudi Arabia*

[e] *Glasgow College, University of Electronic Science and Technology of China, Chengdu 610056, China*

[f] *Center of Excellence for Advanced Materials Research, King Abdulaziz University, Jeddah, Saudi Arabia*

[g] *Department of Chemical Engineering, Pohang University of Science and Technology (POSTECH), Pohang 37673, Republic of Korea*

[h] *POSCO-POSTECH-RIST Convergence Research Center for Flat Optics and Metaphotonics, Pohang 37673, Republic of Korea*

[i] *National Institute of Nanomaterials Technology (NINT), Pohang 37673, Republic of Korea*

† Electronic supplementary information (ESI) available. See DOI: https://doi.org/10.1039/d2nh00555g

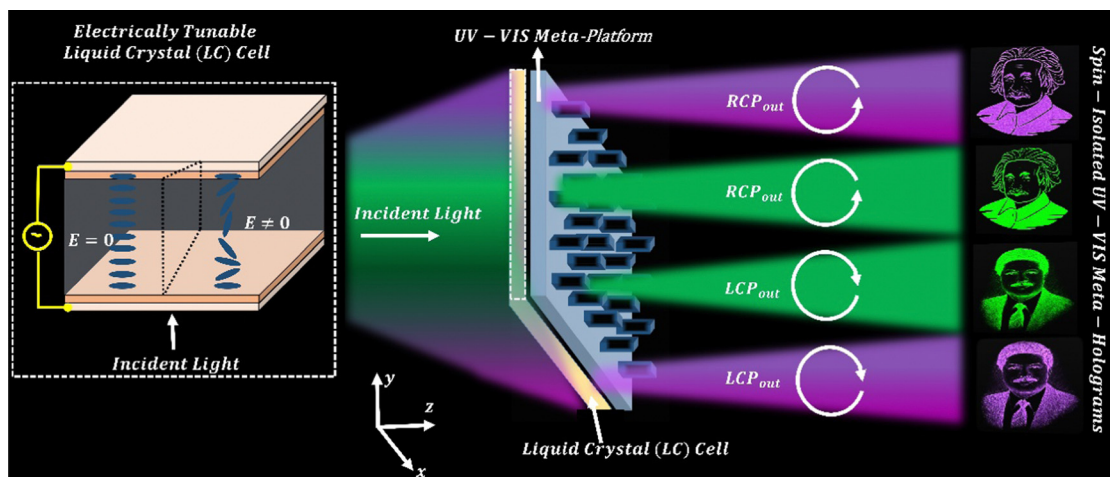‡ A. A., J. K. and H. S. K. contributed equally to this work.

Fig. 1 Artistic view of the working principle of the proposed platform. The proposed meta-platform integrated with a liquid crystal (LC) provided dynamic spin-isolated meta-holograms at broadband wavelengths in UV and visible regimes. The inset shows the electrically tunable LC cell with linearly polarized light illumination.

them to outperform conventional optical components.[1–9] Metasurfaces have previously been shown to constitute an efficient and compact solution for meta-holographic displays.[10–14] Consequently, on-chip realization of such metasurfaces can provide wearable or head-mounted displays (HMDs) for promising applications in augmented reality (AR) and virtual reality (VR).[15–18] Moreover, such displays have promising applications in healthcare for bio-imaging, the advertisement industry, data encryption, *etc.* In the last decade, metasurfaces have garnered considerable attention for targeting versatile functionalities like vortex beam generation,[19–21] lenses,[21] novel light structuring,[22–30] and color filters.[31–34]

Furthermore, based on design methodologies, numerous metasurfaces have been demonstrated for meta-holographic displays using metallic and dielectric nano-resonators.[35–41] However, dielectrics emerged as the suitable choice to mitigate the limitation of low efficiency in plasmonic-based metasurfaces.[42–46] Then, there were many reports on the construction of meta-holograms in the visible (Vis) and terahertz (THz) regimes.[10,45,47–49] But a few groups have reported metasurfaces at ultraviolet (UV) wavelengths suffering from low efficiency, and the need to contend with costly and complex fabrication procedures.[50–59] For example, a broadband dielectric metasurface comprising silicon (Si) meta-atoms designed at UV wavelengths has been reported to exhibit an efficiency of ∼30%, attributed to the high extinction coefficient in the UV regime.[50]

To overcome this low efficiency, researchers have developed aluminum nitride (Al$_2$N$_3$)-based,[52] niobium pentoxide (Nb$_2$O$_5$)-based,[54] and hafnium dioxide (HfO$_2$)-based[55] metasurfaces in the UV regime. However, such metasurfaces either require complex and costly fabrication or cannot provide high efficiency at deep UV wavelengths. In short, to the best of our knowledge, an all-dielectric, highly efficient single metasurface working in UV-Vis regimes, including the extra degree of freedom to incorporate spin-isolated multiple meta-holographic information, has not been reported yet.

Here, we propose a multi-functional metasurface designed with silicon nitride (Si$_3$N$_4$)-based meta-atoms for the realization of simultaneous conversion of amplitude, polarization, and phase in terms of meta-holographic displays at broadband UV-Vis wavelengths. The high refractive index (n), band gap energy of 5.9 eV, and negligible extinction coefficient (k) of Si$_3$N$_4$ make it transparent for the whole UV regime. Moreover, the proposed metasurface providing fabrication ease with a maximum conversion efficiency in transmission exceeding 80%. Various aspects of the liquid crystal integrated single planar metasurface were characterized numerically and experimentally, including its multi-functionality allowing it to reproduce spin-isolated dynamic holographic information. As a result, it can provide distinct holographic information for right circularly polarized (RCP) light and left circularly polarized (LCP) light with a broadband optical response at UV-Vis wavelengths. An artistic view of the proposed dynamic meta-platform providing holograms at UV-Vis wavelengths is demonstrated in Fig. 1.

Results and discussion

In designing the meta-atom of any metasurface, the key factor is selecting a material with a high refractive index n and low extinction coefficient k to introduce the ability to confine light well enough with low absorption at the working wavelengths. The bandgap energies of the different materials studied in the current work are shown in Fig. 2(a). These energy levels can provide a range of loss-less wavelength or transparent window. The bandgap energy of Si$_3$N$_4$ is higher than those of the other dielectric materials such as Nb$_2$O$_5$, HFO$_2$, and Si, and hence can provide transparency across a wide range of ultraviolet (UV) and visible wavelengths. Al$_3$N$_4$ can provide transparency at deep UV wavelengths, due to its relatively high bandgap, but its fabrication is complex and costly. The anisotropic meta-atom used as the building block of the proposed metasurface is
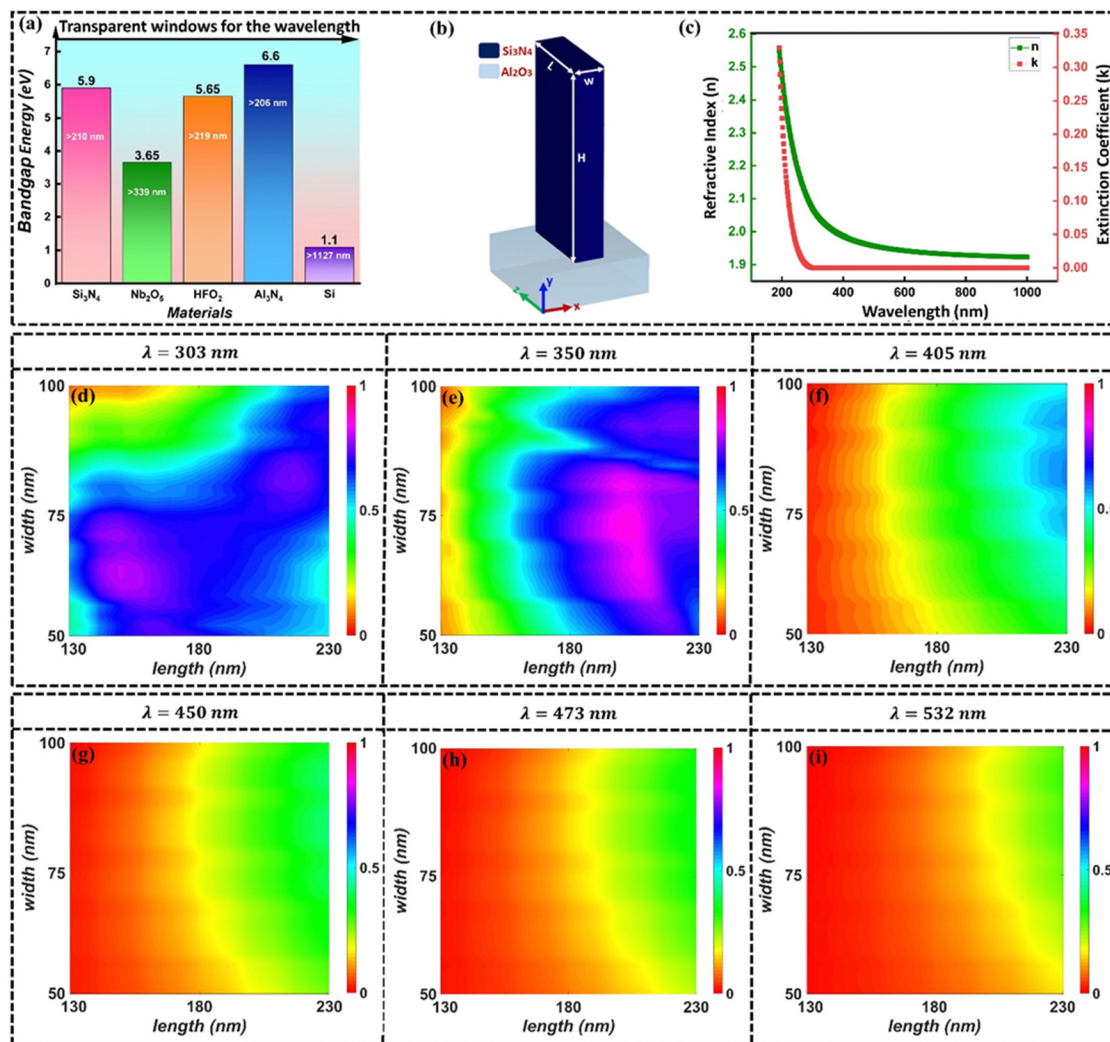
Fig. 2 Design and optimization of meta-atom at broadband UV-Vis wavelengths. (a) Bandgap energy values of silicon nitride (Si₃N₄), niobium pentoxide (Nb₂O₅), hafnium dioxide (HFO₂), aluminum nitride (Al₃N₄), and silicon (Si) to check the transparency window at optical wavelengths. (b) Three-dimensional (3D) view of the meta-atom designed for broadband UV-Vis wavelengths. (c) Plots showing wavelength dependences of refractive index and extinction coefficient of Si₃N₄ used to optimize the meta-atom. (d–i) Cross-polarized transmissions of the meta-atom at wavelengths of (d) 303 nm, (e) 350 nm, (f) 405 nm, (g) 450 nm, (h) 473 nm, and (i) 532 nm.

depicted with its designed parameters in Fig. 2(b). The meta-atom optimized using Si₃N₄ on an Al₂O₃ substrate to provide broadband results covering UV and visible regimes. The refractive index (n) and extinction coefficient (k) of Si₃N₄ are shown in Fig. 2(c).

The simulated cross-polarized transmission efficiency of the meta-atom is depicted in Fig. 2(d)–(i) at UV and visible wavelengths (303 nm, 350 nm, 405 nm, 450 nm, 473 nm, and 532 nm) for a range of length (L) (130–230 nm) and width (W) (50–100 nm). The optimal values of the L and W for maximum transmission at broadband UV-Vis regimes were determined to be 220 nm and 76 nm, respectively.

The simulated transmission conversion efficiency of the optimized meta-atom at broadband UV-Vis wavelengths is depicted in Fig. 3(a). The achieved efficiency exceeded 80% at a wavelength of 350 nm. Meanwhile, full phase coverage (0–2π) was required to reproduce meta-holographic displays. For this purpose, we utilized the geometric phase modulation technique, also

known as the Pancharatnam–Berry (PB) phase, which states that the full phase delay 0–2π can be achieved by rotating the optimized meta-atom in the range 0–π or 0°–180°. The PB phase design methodology can be explained by applying Jones calculus, where the Jones matrix can be described as

$$T = \begin{bmatrix} T_f & 0 \\ 0 & T_s \end{bmatrix} \qquad (1)$$

where T_f and T_s denote the transmission coefficients for the polarized incident light along, respectively, the fast and slow axes of the meta-atom.

The transferred electric field $E(L/R)$ can be expressed as (Section 1 of ESI†)

$$E(L/R) = \frac{T_f + T_s}{2}\hat{e}(L/R) + \frac{T_f + T_s}{2}e^{\pm 2i\varphi}\hat{e}(L/R) \qquad (2)$$
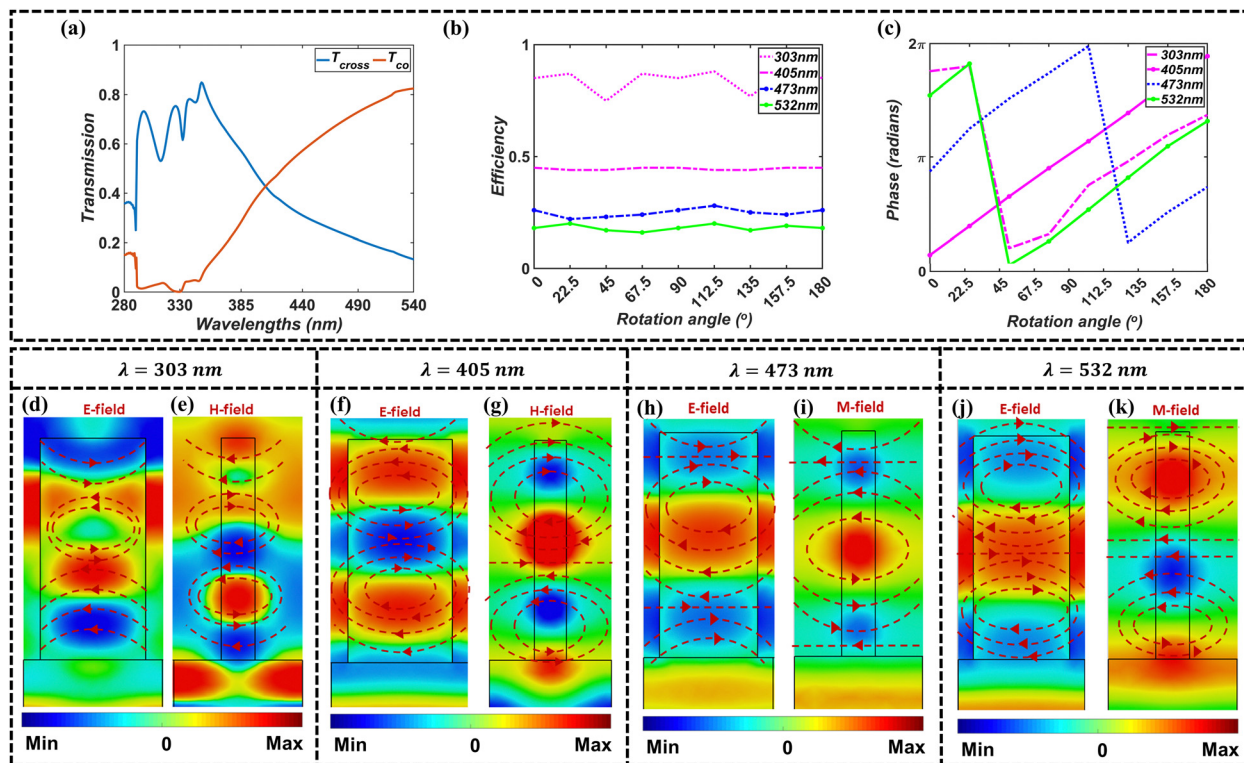
Fig. 3 Optimal conversion efficiency of meta-atom and EM-field profiles. (a) Plots of simulated cross-polarized and co-polarized transmission efficiency values of the meta-atom *versus* UV-Vis wavelength. (b) Plots of cross-polarized transmission *vs.* rotation angle of the meta-atom for geometric phase modulation at working wavelengths. (c) Plots of the geometric phase modulation and full phase coverage at the working wavelengths. (d–k) Simulated electric and magnetic field profiles at wavelengths of, respectively, (d and e) 303 nm, (f and g) 405 nm, (h and i) 473 nm, and (j and k) 532 nm.

In eqn (2), the first term represents the co-polarized transmitted light with no phase change, whereas the second term represents the cross-polarized transmitted light with a phase shift of $\pm 2i\varphi$.

From these formulations, it was determined that the full phase coverage ($0–2\pi$) can be attained by changing the orientation angle of the meta-atom from $0–\pi$.

However, in our case for spin-isolated meta-holography, two distinct phase masks were encoded into the metasurface. This feature incorporating an extra degree of freedom into the optimized meta-atoms, to enable the different information to be obtained when illuminated by CP light with different handedness. Consequently, the total phase mask needed to be encoded into the proposed metasurface for forward and backward direction illumination can be expressed as

$$\phi_{\mathrm{T}} = \arg\left[e^{i\phi_{\mathrm{F}}}\right] + \arg\left[e^{-i\phi_{\mathrm{B}}}\right] \qquad (3)$$

where ϕ_{T}, ϕ_{F} and ϕ_{B} denote the total phase and phases for the forward and backward direction illuminations, respectively.

The total phase profile encoded into the metasurface can be written as in eqn (4) (Section 1: ESI†),

$$\phi_{\mathrm{T}} = \arg\left[e^{i\left(\tan^{-1}\{\tan(A)\}\right)}\right] \qquad (4)$$

where $A = \dfrac{\phi_{\mathrm{F}} - \phi_{\mathrm{B}}}{2}$ eqn (4) was used to implement the spin-isolated phase profiles of two different pieces of information

into a single metasurface for broadband UV-Vis dynamic meta-holographic displays.

For each of the working wavelengths of the UV and visible regimes, transmission conversion efficiency and phase as a function of rotation angle of the meta-atom are depicted in Fig. 3(b) and (c), respectively. The electric and magnetic dipole resonances are depicted in Fig. 3(d)–(k) at the working wavelength of 303 nm, 405 nm, 473 nm, and 532 nm, respectively. The strong field confinements validated the optimization of the meta-atom at the broadband UV-Vis wavelengths.

The optimized meta-atom was used to design a metasurface for spin-encrypted UV-Vis meta-holography. Computer-generated holograms of images of two renowned scientists (Albert Einstein and Ahmed Hassan Zewail) are depicted in Fig. 4(a). We thank Won Jun Choi for designing the image of Ahmed Hassan Zewail for our use in this holography work. For each image, the phase mask was embedded into the designed metasurface. The process for fabricating the proposed UV-Vis metasurface started with the deposition of a 500-nm-thick layer of Si_3N_4 on a glass substrate using plasma-enhanced chemical vapor deposition (PECVD). Then, a chromium (Cr) layer with a thickness of 70 nm was deposited on Si_3N_4 using electron beam evaporation, acting as an etching mask. Next, acetone was used to lift off the Cr, and the Cr patterns were transferred onto the Si_3N_4 layer using a dry etching process. Meanwhile, Cr etchant (CR-7) was used to remove the remaining Cr etching mask. A schematic of the fabrication process is shown in Fig. S1 (Section 2: ESI†).
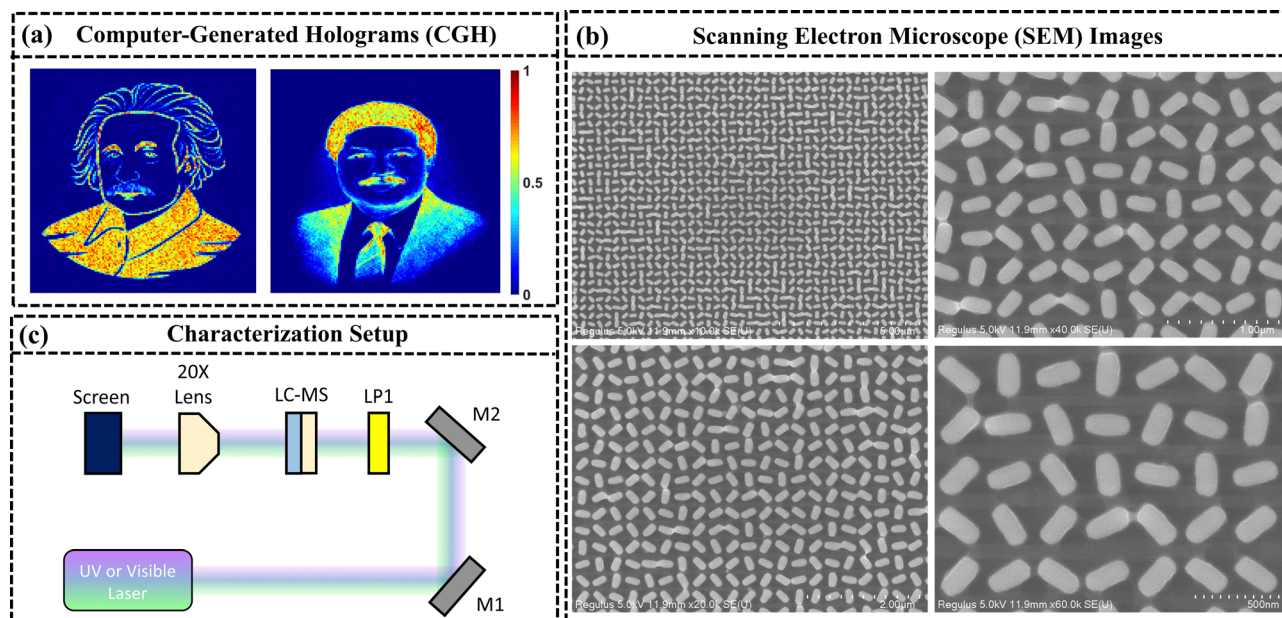
Fig. 4 Fabrication and characterization of UV–Vis meta-platform. (a) Computer-generated holograms of images of two renowned Nobel Prize-winning scientists (Albert Einstein and Ahmed Hassan Zewail) encoded into the spin-encrypted UV–Vis meta-platform. (b) SEM images of the fabricated meta-platform for dynamic meta-holographic displays. (c) Schematic of the characterization setup of the designed meta-platform integrated with a liquid crystal (LC). UV and visible lasers at multiple wavelengths for broadband analysis were used as the light source. The light beam from the laser reflected by the mirrors (M1 and M2) illuminated the LC-integrated meta-platform (LC-MS) after passing through the linear polarizer (LP1). The light beam from LC-MS was observed at the objective lens (20× lens) to focus the reproduced hologram image on a display screen.

The scanning electron microscope (SEM) images acquired of a small portion of the fabrication device are depicted in Fig. 4(b). The total size of the fabricated device was 500 × 500 μm². Fig. 4(c) illustrates the characterization setup for the fabricated UV-Vis meta-platform. UV and visible lasers were used as the light source to illuminate the fabricated sample. The light beam from the laser source was reflected by the mirrors (M1 and M2) and, after passing through the linear polarizer (LP1), illuminated the liquid crystal (LC)-integrated meta-platform (LC-MS). The light beam from the LC-MS was observed at the objective lens (20x lens) to focus the reproduced hologram images. The visible light was captured on the screen, and a UV sensor card was used to capture the UV light.

Fig. 5a depicts the electrically tunable LC cell used to control the polarization of incident linearly polarized light. The LC-integrated fabricated sample provided the ability to reproduce spin-isolated and dynamic holograms in UV and visible regimes. The absorbance spectra acquired for the used LC cell are depicted in Fig. S2 (Section 3: ESI†). The experimental results obtained at the UV (325 nm and 405 nm) and visible wavelengths (473 nm and 532 nm) are depicted in Fig. 5(b). For LCP illumination, the meta-platform was used to reproduce the hologram of Albert Einstein at the working wavelengths in the UV and visible regimes. In contrast, changing the polarization of incident light into RCP was carried out to generate a hologram of Ahmed Hassan Zewail. The measured results at the wavelength of 450 nm are depicted in Fig. S3 (Section 4: ESI†). The dynamic generation of spin-isolated holograms with good fidelity proved the concept of multifunctionality at broadband wavelengths in

UV and visible regimes. The conversion efficiency values for holograms at multiple wavelengths in the UV and visible regimes are shown in Fig. 5(c), with a maximum efficiency of ∼43% at 325 nm and minimum efficiency of ∼16% at 532 nm. The conversion efficiency was calculated using the formulation given in eqn (5).

$$\text{Converison efficiency} = \frac{P_{\text{out}}}{P_{\text{in}}} \times 100 \qquad (5)$$

Conclusions

Here, a multi-functional planar dielectric metasurface integrated with a liquid crystal was demonstrated numerically and experimentally to reproduce spin-isolated dynamic holographic information at broadband UV-Vis wavelengths. The proposed metasurface incorporated two holographic phase profiles using a geometric phase modulation technique with silicon nitride (Si$_3$N$_4$) meta-atoms. The high refractive index (n) of Si$_3$N$_4$ with a band gap energy of 5.9 eV and negligible extinction coefficient (k) made it transparent for the whole UV regime. Hence, the proposed single-layer metasurface provided for ease of fabrication with a high transmission conversion efficiency at broadband UV-Vis wavelengths with a maximum conversion efficiency of ∼80% at a wavelength of 350 nm. Moreover, it provided distinct holographic information for right circularly polarized (RCP) and left circularly polarized (LCP) light with the broadband optical response in UV-Vis regimes. Such metasurfaces incorporating multiple pieces of holographic information with polarization-dependent responses
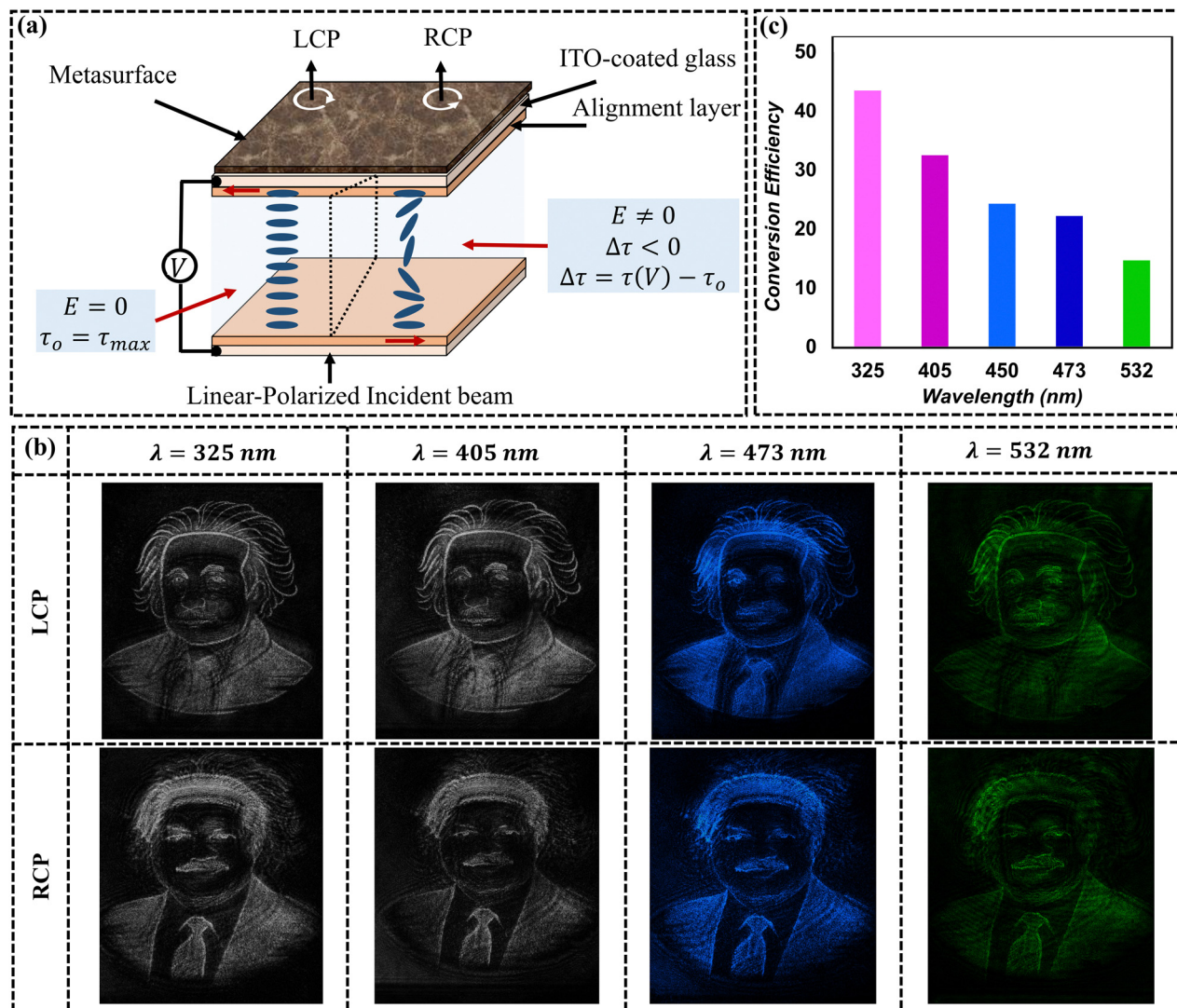
Fig. 5 Experimental demonstration of fabricated UV-Vis meta-platform. (a) Schematic of the electrically tunable LC cell integrated with the fabricated meta-platform and behaving as the polarization regulator for dynamic holographic displays. The LC controlled the polarization of incident light to generate the LCP and RCP light. (b) Measured results at the working wavelengths of 325 nm, 405 nm, 473 nm, and 532 nm in the UV and visible regimes. For LCP illumination, the encrypted meta-platform reproduced the encoded image of Albert Einstein, whereas the image of Ahmed Hassan Zewail was generated using RCP incident light. (c) Conversion efficiency values of the reproduced holograms at the UV and visible wavelengths.

can be integrated with AR technology and have promising applications in optical security encryption, anti-counterfeiting, UV nanophotonics, advertisements, the media industry, and specifically in the healthcare sector.[15,17]

Author contributions

All authors have approved the final version of the manuscript. Conceptualization, J. R., Y. M., M. Q. M.; methodology, A. A., J. K., H. S. K.; software, A. A.; validation, N. M., J. A., M. T. S. C., M. Z.; formal analysis, J. K., Y. K., D. J.; investigation, A. A., J. K., H. S. K.; resources, N. M., J. A., M. T. S. C., M. Z.; data curation, J. K., Y. K., D. J.; writing – original draft, A. A., J. K., H. S. K.; writing – review & editing, J. R., Y. M., M. Q. M., M. Z.; visualization, A. A., J. K., H. S. K.; supervision, J. R., Y. M.,

M. Q. M.; project administration, J. R., Y. M., M. Q. M.; funding acquisition, J. R.

Conflicts of interest

The authors declare no competing interests.

Acknowledgements

References

1 N. Yu and F. Capasso, *Nat. Mater.*, 2014, **13**, 139–150.

2 S. A. Maier, *Plasmonics: fundamentals and applications*, Springer, 2007.

3 W. Cai and V. M. Shalaev, *Optical metamaterials*, Springer, 2010.

4 A. V. Kildishev, A. Boltasseva and V. M. Shalaev, *Science*, 2013, **339**, 1232009.

5 N. Yu, P. Genevet, M. A. Kats, F. Aieta, J.-P. Tetienne, F. Capasso and Z. Gaburro, *Science*, 2011, **334**, 333–337.

6 D. Lee, S. So, G. Hu, M. Kim, T. Badloe, H. Cho, J. Kim, H. Kim, C.-W. Qiu and J. Rho, *eLight*, 2022, **2**, 1.

7 L. Li, H. Zhao, C. Liu, L. Li and T. J. Cui, *eLight*, 2022, **2**, 7.

8 R. Zhu, J. Wang, T. Qiu, Y. Han, X. Fu, Y. Shi, X. Liu, T. Liu, Z. Zhang, Z. Chu, C.-W. Qiu and S. Qu, *eLight*, 2022, **2**, 10.

9 N. Mahmood, J. Kim, M. A. Naveed, Y. Kim, J. Seong, S. Kim, T. Badloe, M. Zubair, M. Q. Mehmood, Y. Massoud and J. Rho, *Nano Lett.*, 2023, **23**, 1195–1201.

10 S. S. Bukhari, J. Vardaxoglou and W. Whittow, *Appl. Sci.*, 2019, **9**, 2727.

11 M. Khorasaninejad, A. Ambrosio, P. Kanhaiya and F. Capasso, *Sci. Adv.*, 2016, **2**, e1501258.

12 H. S. Khaliq, I. Kim, J. Kim, D. K. Oh, M. Zubair, K. Riaz, M. Q. Mehmood and J. Rho, *Adv. Opt. Mater.*, 2021, **9**, 2002002.

13 D. Wen, F. Yue, G. Li, G. Zheng, K. Chan, S. Chen, M. Chen, K. F. Li, P. W. H. Wong, K. W. Cheah, E. Yue Bun Pun, S. Zhang and X. Chen, *Nat. Commun.*, 2015, **6**, 8241.

14 S. So, J. Kim, T. Badloe, C. Lee, Y. Yang, H. Kang and J. Rho, *Adv. Mater.*, 2023, **35**, 2208520.

15 J.-H. Park and B. Lee, *Light: Adv. Manuf.*, 2022, **3**, 9.

16 T. Jung and M. C. Tom Dieck, *Augmented Reality and Virtual Reality Empowering Human, Place and Business*, Springer International Publishing AG, 2018.

17 C. Plotzky, U. Lindwedel, A. Bejan, P. König and C. Kunze, *i-com*, 2021, **20**, 73–83.

18 J. Kim, J. Seong, W. Kim, G.-Y. Lee, S. Kim, H. Kim, S.-W. Moon, D. K. Oh, Y. Yang, J. Park, J. Jang, Y. Kim, M. Jeong, C. Park, H. Choi, G. Jeon, K.-I. Lee, D. H. Yoon, N. Park, B. Lee, H. Lee and J. Rho, *Nat. Mater.*, 2023, **22**, 474–481.

19 R. C. Devlin, A. Ambrosio, N. A. Rubin, J. P. B. Mueller and F. Capasso, *Science*, 2017, **358**, 896–901.

20 S. Mei, M. Q. Mehmood, S. Hussain, K. Huang, X. Ling, S. Y. Siew, H. Liu, J. Teng, A. Danner and C.-W. Qiu, *Adv. Funct. Mater.*, 2016, **26**, 5255–5262.

21 Z. Jin, D. Janoschka, J. Deng, L. Ge, P. Dreher, B. Frank, G. Hu, J. Ni, Y. Yang, J. Li, C. Yu, D. Lei, G. Li, S. Xiao, S. Mei, H. Giessen, F. M. Zu Heringdorf and C.-W. Qiu, *eLight*, 2021, **1**, 5.

22 H. S. Khaliq, J. Kim, T. Naeem, K. Riaz, T. Badloe, J. Seong, J. Akbar, M. Zubair, M. Q. Mehmood, Y. Massoud and J. Rho, *Adv. Opt. Mater.*, 2022, **10**, 2201175.

23 H. S. Khaliq, I. Kim, A. Zahid, J. Kim, T. Lee, T. Badloe, Y. Kim, M. Zubair, K. Riaz, M. Q. Mehmood and J. Rho, *Photonics Res.*, 2021, **9**, 1667–1674.

24 M. A. Naveed, J. Kim, M. A. Ansari, I. Kim, Y. Massoud, J. Kim, D. K. Oh, T. Badloe, J. Lee, Y. Kim, D. Jeon, J. Choi, M. Zubair, M. Q. Mehmood and J. Rho, *ACS Appl. Mater. Interfaces*, 2022, **14**, 31194–31202.

25 M. A. Abbas, J. Kim, A. S. Rana, I. Kim, B. Rehman, Z. Ahmad, Y. Massoud, J. Seong, T. Badloe, K. Park, M. Q. Mehmood, M. Zubair and J. Rho, *Nanoscale*, 2022, **14**, 6425–6436.

26 H. S. Khaliq, I. Kim, K. Riaz, T. Naeem, M. Zubair, J. Rho and M. Q. Mehmood, *J. Phys.: Conf. Ser.*, 2021, **2015**, 012060.

27 H. S. Khaliq, M. R. Akram, K. Riaz, M. A. Ansari, J. Akbar, J. Zhang, W. Zhu, D. Zhang, X. Wang, M. Zubair and M. Q. Mehmood, *Opt. Express*, 2021, **29**, 3230–3242.

28 M. A. Naveed, J. Kim, I. Javed, M. A. Ansari, J. Seong, Y. Massoud, T. Badloe, I. Kim, K. Riaz, M. Zubair, M. Q. Mehmood and J. Rho, *Adv. Opt. Mater.*, 2022, **10**, 2200196.

29 J. Kim, Y. Yang, T. Badloe, I. Kim, G. Yoon and J. Rho, *InfoMat*, 2021, **3**, 739–754.

30 J. Kim, D. K. Oh, H. Kim, G. Yoon, C. Jung, J. Kim, T. Badloe, H. Kang, S. Kim, Y. Yang, J. Lee, B. Ko, J. G. Ok and J. Rho, *Laser Photonics Rev.*, 2022, **16**, 2200098.

31 Y.-S. Lin, J. Dai, Z. Zeng and B.-R. Yang, *Nanoscale Res. Lett.*, 2020, **15**, 77.

32 C.-S. Park, V. R. Shrestha, W. Yue, S. Gao, S.-S. Lee, E.-S. Kim and D.-Y. Choi, *Sci. Rep.*, 2017, **7**, 2556.

33 T. Badloe, J. Kim, I. Kim, W.-S. Kim, W. S. Kim, Y.-K. Kim and J. Rho, *Light: Sci. Appl.*, 2022, **11**, 118.

34 T. Lee, J. Kim, I. Koirala, Y. Yang, T. Badloe, J. Jang and J. Rho, *ACS Appl. Mater. Interfaces*, 2021, **13**, 26299–26307.

35 T. Badloe, J. Lee, J. Seong and J. Rho, *Adv. Photonics Res.*, 2021, **2**, 2000205.

36 H.-H. Hsiao, C. H. Chu and D. P. Tsai, *Small Methods*, 2017, **1**, 1600064.

37 Z.-L. Deng, M. Jin, X. Ye, S. Wang, T. Shi, J. Deng, N. Mao, Y. Cao, B.-O. Guan, A. Alù, G. Li and X. Li, *Adv. Funct. Mater.*, 2020, **30**, 1910610.

38 S. M. Kamali, E. Arbabi, A. Arbabi and A. Faraon, *Nanophotonics*, 2018, **7**, 1041–1068.

39 F. Zhou, Y. Liu and W. Cai, *Opt. Express*, 2013, **21**, 4348–4354.

40 Y.-W. Huang, W. T. Chen, W.-Y. Tsai, P. C. Wu, C.-M. Wang, G. Sun and D. P. Tsai, *Nano Lett.*, 2015, **15**, 3122–3127.

41 I. Javed, J. Kim, M. A. Naveed, D. K. Oh, D. Jeon, I. Kim, M. Zubair, Y. Massoud, M. Q. Mehmood and J. Rho, *ACS Appl. Mater. Interfaces*, 2022, **14**, 36019–36026.

42 R. C. Devlin, M. Khorasaninejad, W. T. Chen, J. Oh and F. Capasso, *Proc. Natl. Acad. Sci. U. S. A.*, 2016, **113**, 10473–10478.

43 B. Wang, F. Dong, Q.-T. Li, D. Yang, C. Sun, J. Chen, Z. Song, L. Xu, W. Chu, Y.-F. Xiao, Q. Gong and Y. Li, *Nano Lett.*, 2016, **16**, 5235–5240.

44 W. Zhao, H. Jiang, B. Liu, J. Song, Y. Jiang, C. Tang and J. Li, *Sci. Rep.*, 2016, **6**, 30613.

45 Z. Li, I. Kim, L. Zhang, M. Q. Mehmood, M. S. Anwar, M. Saleem, D. Lee, K. T. Nam, S. Zhang, B. Luk'yanchuk, Y. Wang, G. Zheng, J. Rho and C.-W. Qiu, *ACS Nano*, 2017, **11**, 9382–9389.

46 F. Zhang, M. Pu, X. Li, P. Gao, X. Ma, J. Luo, H. Yu and X. Luo, *Adv. Funct. Mater.*, 2017, **27**, 1704295.

47 G. Yoon, D. Lee, K. T. Nam and J. Rho, *ACS Photonics*, 2018, **5**, 1643–1647.

48 K. Huang, Z. Dong, S. Mei, L. Zhang, Y. Liu, H. Liu, H. Zhu, J. Teng, B. Luk'yanchuk, J. K. W. Yang and C.-W. Qiu, *Laser Photonics Rev.*, 2016, **10**, 500–509.

49 B. Wang, B. Quan, J. He, Z. Xie, X. Wang, J. Li, Q. Kan and Y. Zhang, *Sci. Rep.*, 2016, **6**, 35657.

50 Y. Deng, X. Wang, Z. Gong, K. Dong, S. Lou, N. Pégard, K. B. Tom, F. Yang, Z. You, L. Waller and J. Yao, *Adv. Mater.*, 2018, **30**, 1802632.

51 X. Gao, R. Wan, J. Yan, L. Wang, X. Yi, J. Wang, W. Zhu and J. Li, *Appl. Opt.*, 2020, **59**, 4398–4403.

52 L. Guo, Z. Hu, R. Wan, L. Long, T. Li, J. Yan, Y. Lin, L. Zhang, W. Zhu and L. Wang, *Nanophotonics*, 2019, **8**, 171–180.

53 K. Huang, J. Deng, H. S. Leong, S. L. K. Yap, R. B. Yang, J. Teng and H. Liu, *Laser Photonics Rev.*, 2019, **13**, 1800289.

54 Z. Zhang, T. Li, X. Jiao, G. Song and Y. Xu, *Appl. Sci.*, 2020, **10**, 5716.

55 C. Zhang, S. Divitt, Q. Fan, W. Zhu, A. Agrawal, Y. Lu, T. Xu and H. J. Lezec, *Light: Sci. Appl.*, 2020, **9**, 55.

56 Z. Hu, L. Long, R. Wan, C. Zhang, L. Zhang, J. Yan, H. Duan and L. Wang, *Opt. Lett.*, 2020, **45**, 3466–3469.

57 D. Zhao, Z. Lin, W. Zhu, H. J. Lezec, T. Xu, A. Agrawal, C. Zhang and K. Huang, *Nanophotonics*, 2021, **10**, 2283–2308.

58 J. Kim, D. Jeon, J. Seong, T. Badloe, N. Jeon, G. Kim, J. Kim, S. Baek, J.-L. Lee and J. Rho, *ACS Nano*, 2022, **16**, 3546–3553.

59 J. Kim, W. Kim, D. K. Oh, H. Kang, H. Kim, T. Badloe, S. Kim, C. Park, H. Choi, H. Lee and J. Rho, *Light: Sci. Appl.*, 2023, **12**, 68.

This journal is © The Royal Society of Chemistry 2023